

Numerical Simulation of Performance of an Axial Turbine First Stage

Vinicius Guimarães Monteiro^{1,*}, Edson Luiz Zapparoli¹, Cláudia Regina de Andrade¹, Rosiane Cristina de Lima²

¹Instituto Tecnológico de Aeronáutica – São José dos Campos/SP – Brazil

²Vale Soluções em Energia – São José dos Campos/SP – Brazil

Abstract: This work has presented the first stage performance at design and off-design operating points of an axial turbine, with two stages using a numerical simulation. Experimental methods of predicting the performance of axial turbine is costly and time consuming compared to the computational fluid dynamics approach. Therefore, computational techniques were adopted to determine the stage performance. This study analyzed the first stage performance of an axial flow turbine, using a computational tool for simulating the steady state two/three-dimensional viscous flow. A computational fluid dynamics software was used to solve the rans equations with the spalart-allmaras turbulence model. The computational fluid dynamics results were compared with those obtained from the mean line loss model code. The comparisons have been conducted to provide a pretest performance for the turbine first stage.

Keywords: Axial Turbines, Gas Turbines, Computational Fluid Dynamics, Numerical Simulation, Performance.

LIST OF SYMBOLS

H :	Total enthalpy	ρ :	Density
S :	Scalar measure of the deformation tensor	$\bar{\tau}_{ij}$:	Shear stress tensor
T :	Temperature	χ :	Intermediate variable
T_2 :	Temperature at exit of stage	$\bar{\Phi}$:	Reynolds average of a generic variable
d :	Distance from the wall	$\tilde{\Phi}$:	Favre average of a generic variable
f_{v1}, f_{v2}, f_w :	Empirical functions in the turbulence model	Φ' :	Time average of variable $\bar{\Phi}$
k :	Coefficient of thermal conductivity	Φ'' :	Time average of variable $\tilde{\Phi}$
K :	Constant in the turbulence model	i, j, k :	Unit vector in a Cartesian coordinate system
p :	Pressure	in, out :	Inlet and exit conditions
s :	Specific entropy	θ :	Stagnation value
t :	Time		
u :	Velocity component in a Cartesian system		
x :	Cartesian coordinate		
g, r, \tilde{S} :	Intermediate variables		
ζ :	Energy loss coefficient in the entropy form		
η :	Total efficiency		
μ :	Dynamic viscosity		
ν :	Kinematic molecular viscosity		

INTRODUCTION

In the past, the experimental method was the single tool adopted to understand with details and to visualize some source loss that occur along the fluid flow. With the appearance of computational techniques in the last 40 years, another alternative emerged to analyze the fluid flow: the numerical simulation. The accuracy of the Computational Fluid Dynamics (CFD) predictions of turbomachinery component efficiency at the design point is around $\pm 2\%$, if one takes into account uncertainty in the numerical methods, models, geometry,

Received: 16/11/11 Accepted: 15/02/12

*author for correspondence: viniciusgm@gmail.com

Pç. Mal. Eduardo Gomes, 50. CEP: 12.228-901

São José dos Campos/SP – Brazil

and boundary conditions (Denton and Xu, 2002). Commonly designers adopt this approach to investigate the fluid flow and to choose experiments to be performed (Fortuna, 2000). Computational techniques are less costly and time-consuming if compared to the experimental approach to predict the performance of the axial turbine (Fletcher, 1991).

Dorney (2003) conducted a pretest performance for a two-stage supersonic turbine. The objective of the work was to quantify the performance of the turbine at off- design flow conditions, as well as to characterize changes in the unsteadiness as a function of flow condition. The simulations were performed using a three-dimensional unsteady Navier-Stokes equation. The predicted results were compared with solutions from a mean-line code. This code uses a combination of the one-dimensional equations of motion and empirical loss models to predict the flow and performance quantities in the turbine. The results showed reasonable agreement over a wide range of flow conditions, and they were used to help determining the locations of the transducers in the experiments.

Welch (2011) developed the three-dimensional (3D) aerodesign and analyzed the relevant stage of an aeronautical turbine component at a level sufficient to verify that the design and off-design performances of the 3D computational results are consistent with the mean line analysis used in the conceptual design of the turbine. The author reports that 3D flow features associated with transport, due to radial acceleration fields and cross-passage gradients, would lead to higher losses than predicted by the mean line loss correlations and two-dimensional (2D) CFD analyses. It was concluded that the 3D computational results yield good agreement with the predicted ones by the mean line analyses showed from efficiency versus speed trends, supporting the design choice to execute the turbine design at the cruise operating speed.

Saravanamutto (1992), in a work published at AGARD-LS-183 report, explained that the steady state prediction of performance must be done at the beginning of an engine development program, in order to ensure that the engine can satisfy all the operation requirements (design and off-design points). Thus, the component characteristics must be estimated and then updated as the program unfolds.

This study deals with steady state 2/3D viscous flow to obtain information about the performance of a first-stage axial turbine by simulating the flow through the blades. A commercial software package was used to solve the RANS equations with the Spalart-Allmaras turbulence model. Despite of 2D CFD approach limitations, it is important to

evaluate differences between 2D and 3D approach results. The key objective of the present effort was to conduct a pretest performance for a first-stage turbine at a level sufficient to verify if the CFD results are consistent with the classical loss model and mean line analysis. To achieve the objective, it was constructed a performance map for the whole range of operation of turbine. The CFD results were compared with the mean line loss model code ones, which account the losses by Denton loss model. Furthermore, it will be presented the Mach number and total pressure from hub to tip of stator blade and rotor blade in the region near the leading and trailing edges. The comparison of these parameters calculated by the 3D CFD simulations was made against mean line loss model code results generated by the manufacturer. The comparisons have been conducted to verify if the 3D CFD results are consistent with the mean line analysis used in the conceptual design of the turbine.

COMPUTATIONAL METHODOLOGY

Conservation equations

The flow field was modeled using the Reynolds Averaged Navier-Stokes Equations (Tannehill *et al.*, 1997), as can be seen in Eq. 1 to 3.

- Continuity equation:

$$\frac{\partial \bar{\rho}}{\partial t} + \frac{\partial}{\partial x_j} (\bar{\rho} \tilde{u}_j) = 0. \quad (1)$$

- Momentum equation:

$$\begin{aligned} \frac{\partial}{\partial t} (\bar{\rho} \tilde{u}_i) + \frac{\partial}{\partial x_j} (\bar{\rho} \tilde{u}_i \tilde{u}_j) \\ = - \frac{\partial \bar{p}}{\partial x_i} + \frac{\partial}{\partial x_j} (\bar{\tau}_{ij} - \overline{\rho u_i'' u_j''}). \end{aligned} \quad (2)$$

- Energy equation:

$$\begin{aligned} \frac{\partial}{\partial t} (\bar{\rho} \tilde{H}) + \frac{\partial}{\partial x_j} \left(\bar{\rho} \tilde{u}_j \tilde{H} + \overline{\rho u_j'' H''} - k \frac{\partial \bar{T}}{\partial x_j} \right) \\ = \frac{\partial \bar{p}}{\partial t} + \frac{\partial}{\partial x_j} (\tilde{u}_i \bar{\tau}_{ij} + \overline{u_i'' \tau_{ij}}). \end{aligned} \quad (3)$$

TURBULENCE MODEL

The choice of turbulence model is a factor that influences the numerical simulation accuracy of the flow through turbine blades (Pecnik *et al.*, 2005). The Spalart-Allmaras turbulence model was adopted in this study, because it was developed primarily for aerodynamic flow (Javaherchi, 2010), and it presents good performance in adverse pressure gradient regions (Menter, 2003). The model requires moderate computational cost to solve the viscous sub-layer (Eulitz and Engel, 1997).

Spalart and Allmaras (1992) proposed to close the system of equations, introducing eight closure coefficients and three closure functions. The model is written in terms of modified eddy viscosity ($\tilde{\nu}$) (Wilcox, 1993). The equations of the Spalart-Allmaras turbulence model are expressed by Eq. 4 to 10:

- Kinematic Eddy viscosity:

$$\frac{\mu_t}{\rho} = \nu_t, \quad \nu_t = \tilde{\nu} f_{\nu 1}. \quad (4)$$

- Eddy viscosity equation:

$$\begin{aligned} \frac{\partial \tilde{\nu}}{\partial t} + U_j \frac{\partial \tilde{\nu}}{\partial x_j} = c_{b1} \tilde{S} \tilde{\nu} - c_{w1} f_w \left(\frac{\tilde{\nu}}{d} \right)^2 \\ + \frac{1}{\sigma} \frac{\partial}{\partial x_k} \left[(\nu + \tilde{\nu}) \frac{\partial \tilde{\nu}}{\partial x_k} \right] + \frac{c_{b2}}{\sigma} \frac{\partial \tilde{\nu}}{\partial x_k} \frac{\partial \tilde{\nu}}{\partial x_k} \end{aligned} \quad (5)$$

- Closure coefficients:

$$c_{b1} = 0,1355, \quad c_{b2} = 0,622, \quad c_{\nu 1} = 7,1, \quad \sigma = 2/3 \quad (6)$$

$$c_{w1} = \frac{c_{b1}}{k^2} + \frac{(1 + c_{b2})}{\sigma}, \quad c_{w2} = 0,3, \quad c_{w3} = 2, \quad k = 0,41 \quad (7)$$

- Auxiliary relations:

$$f_{\nu 1} = \frac{X^3}{X^3 + c_{\nu 1}^3}, \quad f_{\nu 2} = 1 - \frac{X}{1 + X f_{\nu 1}}, \quad f_w = g \left(\frac{1 + c_{w3}^6}{g^6 + c_{w3}^6} \right)^{\frac{1}{6}} \quad (8)$$

$$X = \frac{\tilde{\nu}}{\nu}, \quad g = r + c_{w2} (r^6 - r), \quad r = \frac{\tilde{\nu}}{\tilde{S} k^2 d^2} \quad (9)$$

$$\tilde{S} = S + \frac{\tilde{\nu}}{k^2 d^2} f_{\nu 2}, \quad S = \sqrt{2 \Omega_{ij} \Omega_{ij}} \quad (10)$$

The tensor $\Omega_{ij} = \frac{1}{2} \left(\frac{\partial U_i}{\partial x_j} - \frac{\partial U_j}{\partial x_i} \right)$ is the rotation tensor and d is the distance from the closest surface.

BOUNDARY CONDITIONS

The 2D simulation was made at mean line of the first stage channel. The total conditions of pressure and temperature at inlet were considered. At the outlet, the static pressure was fixed. Periodicity regions were considered at the interblade positions. At the spaces between consecutive rows, frozen rotor approach was adopted. The periodicity of stator-rotor blades is solved by a domain scale, as discussed by Murari *et al.* (2011) and Toussaint *et al.* (1997), which results in five stator blade rows and eight rotor blade rows. The stationary conditions to the absolute reference frame were applied to the stator blades. The rotor blades have translational velocity of 367 m/s on the design point.

The 3D simulation was made at only one blade passage. This was possible because the mixing plane averages were adopted at the space between consecutive rows. Using the frozen rotor approach for 3D model excessively increases the computational cost, due to the numbers of blade rows necessary to satisfy the periodicity of stator-rotor blades. For this reason, it was chosen the mixing plane approach in the stage interfaces for 3D model. Total pressure and total temperature at inlet were considered. At outlet, the static pressure was fixed. Periodicity regions were considered at the interblade positions. The stationary condition to the absolute reference frame was applied to the stator blade. The rotor blade has rotational velocity of 22,600 rpm on design point. Tip leakage was not considered.

The boundary conditions used in the inlet and outlet of 2D and 3D models in the design point are presented in Table 1.

Table 1. Inlet and outlet boundary conditions.

Total pressure inlet	587,745.8 Pa
Total temperature inlet	1,100 K
Static pressure outlet	229,449 Pa
Turbulent intensity inlet	5%

The walls for 2D and 3D approaches are adiabatic and non-slip conditions were adopted. To solve the flow near the wall, the solver applies the law of the wall developed by Launder e Spalding (ANSYS, 2009a, b). This method is not utilized when the values of y^+ are smaller than six for the Spalart-Allmaras turbulence model (ANSYS, 2009a). The law of the wall is applied appropriately to the turbulent boundary layer, when y^+ values are between 20 and 300 (Menter, 2003; ANSYS, 2009a, b).

NUMERICAL METHODS

The 2D approach was simulated by ANSYS Fluent software, version 13.0, which uses the finite-volume discretization method (ANSYS, 2009a). The solver adopted is coupled, implicit, with a time marching to reach the steady state condition, and taking into account the turbulence effects by Spalart-Allmaras one-equation turbulence model.

The 3D approach was simulated by ANSYS CFX software, version 13.0, which employs the finite element-based volume method (ANSYS, 2009b). It was adopted the ANSYS CFX software for the 3D simulation, because the software provides a good pre-processing for solving 3D flow in axial turbomachinery. The solver adopted is coupled, implicit, uses time marching to reach the steady state condition, and solves the turbulence effects by Spalart-Allmaras one-equation turbulence model.

The simulation of compressible flow was smoothly started to avoid numerical instability due to aggressive behavior of this kind of flow inside the turbomachinery. Therefore, it was used a dissipative method by first-order upwind discretization for the convections terms. This method avoids numerical instability due to shock waves.

The flow is not aligned with the mesh (i.e., when it crosses the mesh lines obliquely); however, first-order convective discretization increases the numerical discretization error (numerical diffusion). Therefore, it was used the second-order discretization to obtain more accurate results.

The algebraic multigrid was employed to accelerate the convergence.

MESH GENERATION

The mesh was constructed for two sub-domains, one for stator blade part and other for rotor blade domain.

In the 2D model, the mesh is composed by quadrilaterals elements near to the blade region, in order to capture high gradients normal to the wall. Triangular elements were generated in the rest of the domain. The mesh contains 546,846 elements. The 2D model allows adopting a higher degree of refinement, because it does not increase the computational cost, when comparison is made with the 3D models. The software adopted to construct the mesh demonstrated by Fig. 1 is called Gambit, version 2.4.6.

Figure 1 represents the mesh of all computational domains (left side) and the rotor leading edge (right side).

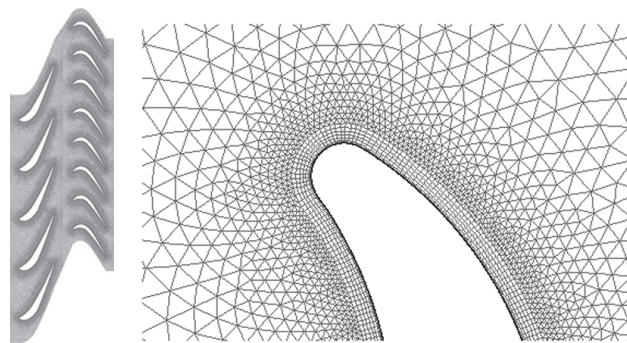


Figure 1. Two-dimensional mesh composed by quadrilateral and triangular elements.

The mesh constructed in the 3D model is composed by tetrahedral in all computational domains. The mesh contains 2,173,242 elements. In the 3D model, the refinement of the mesh increases the computational cost. Therefore, the refinement was made in regions where there are high gradients normal to the wall, such as near the blade walls. Figure 2 shows the 3D mesh constructed using ANSYS ICEM software, version 13.0.



Figure 2. Three-dimensional mesh composed by tetrahedral elements.

MEAN LINE LOSS MODEL CODE

The mean line loss model code uses a combination of the one-dimensional equations of motion in the mean line and empirical loss models to predict the flow and performance quantities in the turbine. Free vortex design techniques and radial equilibrium (Saravanamuttoo *et al.*, 2001) were adopted to find parameters, such as Mach number and total pressure, from hub to tip in regions near the leading and trailing edges of the stator and rotor blades. These parameters were used to verify if the 3D CFD results are consistent with the mean line analysis used by the manufacturer in the conceptual design of

the turbine. The performance quantities, such as the first-stage efficiency of the turbine, were predicted only on design point by the manufacturer using the Kacker-Okapuu loss model. These results will be mentioned in this work as design data.

The performance maps constructed by CFD simulation were verified against results generated by the mean line loss model code, which was developed by Hess (2006), and that adopted Denton loss model. This model is based on results of a large number of cascade tests with specified values of inlet and outlet blade angles, for a given pitch/chord ratio, which results in curves of energy loss coefficients.

Denton (1993) considered that the physical origin of the losses is defined in terms of entropy increase, due to viscous effects in boundary layer, shock waves, heat transfer across temperature differences, and viscous effects in mixing process.

The loss model is established by means of applying boundary layer theories, basic thermodynamic equations, and simplified equation of conservation of mass, momentum and energy on each specific loss condition. Some empirical parameters are also needed for the predictions. In some cases, for instance, attached blade boundary layers, the loss mechanisms are understood, but even so the loss can seldom be predicted with great accuracy. In many other cases, e.g., end-wall loss, the loss mechanisms are still not clearly understood and prediction methods remain very dependent on correlations.

Denton classifies the loss in various forms, such as: trailing edge loss (ζ_{Te}), tip leakage loss (ζ_{Tip}), end-wall boundary layer loss (ζ_{Eb}), shock loss (ζ_{shock}), and profile loss (ζ_p). The sums of all individual losses are accounted as total loss, given by Eq. 11:

$$\zeta = \sum \zeta_i ;$$

$$\zeta = \zeta_p + \zeta_{Te} + \zeta_{Tip} + \zeta_{Eb} + \zeta_{shock} . \quad (11)$$

The creation of entropy by irreversible effects will always reduce the efficiency of a turbine. Hence, the loss of efficiency can be related to the entropy created via eq. 12:

$$\eta = \frac{\Delta H}{(\Delta H + T_2 \Delta s)} . \quad (12)$$

PERFORMANCE MAP

To evaluate the performance of the first-stage turbine, performance maps were constructed, which are the most accurate way for predicting off-design performance (Haglund and Elmergaard, 2009).

However, the off-design performance of an axial turbine is evaluated by performance maps (Saravanamuttoo *et al.*, 2001), which are presented by relations between total efficiency (η_t), pressure ratio (rp), corrected mass flow (m_{corr}), and corrected speed (N_{corr}), given by Eqs. 13 to 16:

$$\eta_t = \frac{H_{in} - H_{out}}{H_{in} - H'_{out}} \quad (13)$$

$$rp = \frac{P_{0in}}{P_{0out}} \quad (14)$$

$$m_{corr} = \frac{\dot{m} \sqrt{T_{0in}}}{T_{0in}} \quad (15)$$

$$N_{corr} = \frac{N}{\sqrt{T_{0in}}} \quad (16)$$

Discussions about the performance map developed in this study will be presented in the next section.

RESULTS AND DISCUSSION

The y^+ values reach the maximum values of four for stator and rotor blades in the 2D simulation, which imply that the law of the wall is not being applied to solve the viscous sub-layer. In the 3D simulation, the mean values of y^+ reach 58 for stator blade and 38 for the rotor blade, which implies that the law of the wall is being appropriately applied to the turbulence boundary layer.

It will be presented, at the design point operation, the Mach number and total pressure distribution. The comparison of these parameters calculated by 3D CFD approach was made against design data.

The mean line analysis represents a good comparison tool to verify the CFD results, as discussed by Dorney (2003) and Welch (2011). It can be noted that all curves (Figs. 3 to 6) present the same general tendency.

The major differences between design data and 3D CFD results can be noted by the behavior of the parameters along the blade span. 3D CFD results presented sharp curves, while the design data have almost linear distribution. These differences can be attributed to the fact that the design data do not take account boundary layers effects, secondary flow, shock waves, and other flow patterns that influence the behavior of the curve.

The presence of secondary flow in the rotor trailing edge causes large variations in the total pressure and Mach number

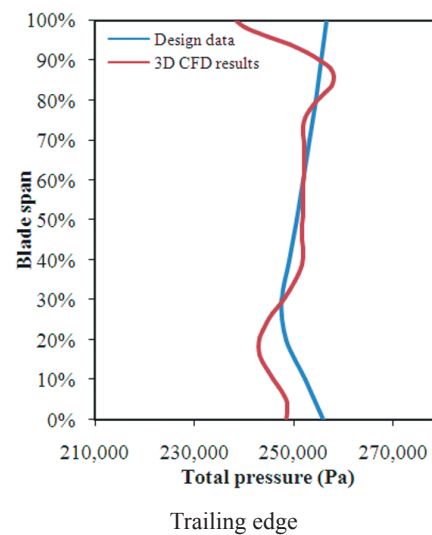
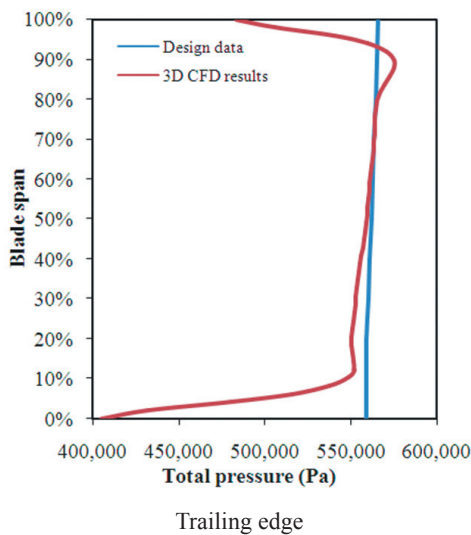
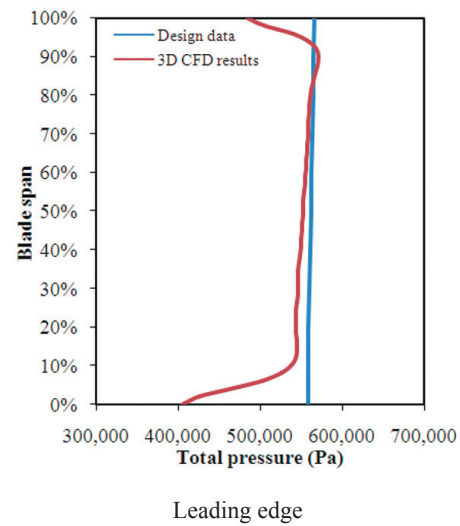
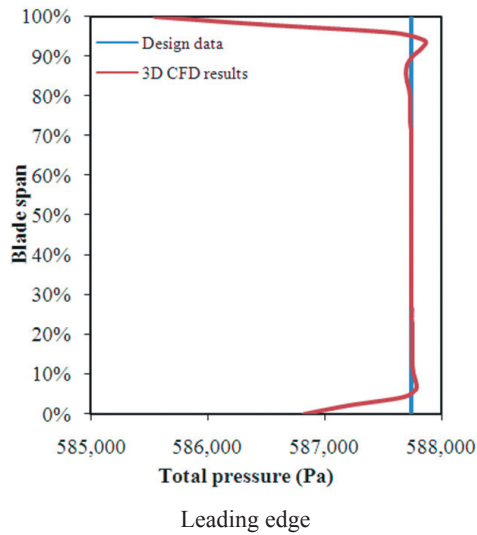


Figure 3. Total pressure distribution at stator blade.

Figure 4. Total pressure distribution at rotor blade.

distribution along the blade span, as mentioned by Tomita and Barbosa (2011). These variations can be viewed by 3D CFD results showed by Figs. 4 and 6.

The boundary layer effects, in the hub and tip of the blade, are shown by the 3D CFD results curves. This behavior can be noted by sharp curves below 10% and above 90% of the blade span.

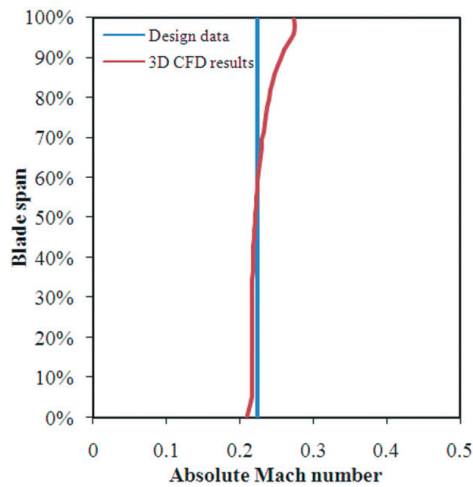
Table 2 presents a comparison of design data against 2D and 3D CFD results for design point operation.

Table 2. Comparison between mass-flow, pressure ratio, and efficiency.

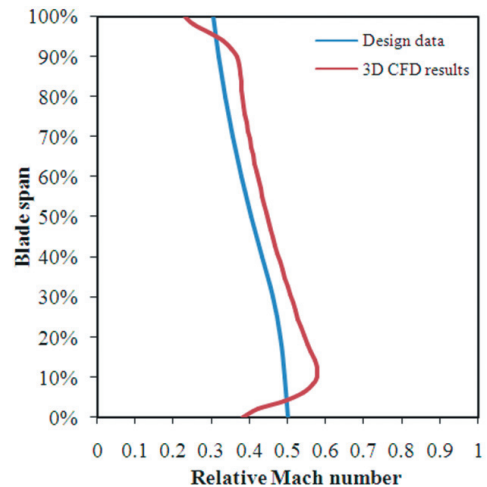
Descriptions	Design data	2D CFD results	Difference (%)	3D CFD results	Difference (%)
Mass-flow (kg/s)	7.12	-	-	6.82	4.21
Pressure ratio	2.56	2.21	13.67	2.35	8.20
Efficiency (%)	86.37	94.25	8.36	85.96	0.47

The mass-flow was not presented to 2D CFD results because the simulation was made in the 2D plane on the 50% of the blade span.

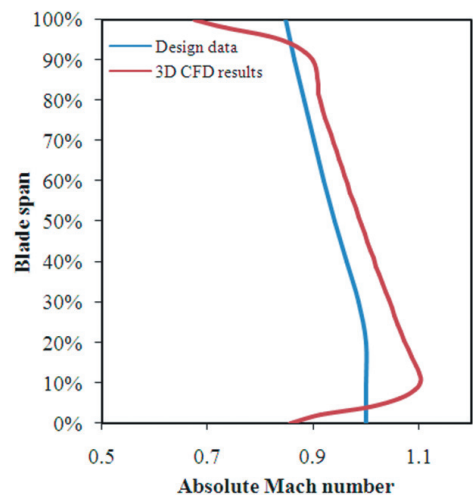
The difference between CFD results and design data is mainly due to one-dimensional characteristic of the mean line analysis, which is not able to capture all flow field details. Similar conclusion can be obtained when comparing 2D and 3D CFD results. The 2D model neglects 3D source-losses due to intrinsic limitations of the model. Some 3D source losses can be explained by the development of boundary layer in the end-wall, and secondary flow in the hub and tip of the blade. The limitations described justify the overestimated efficiency obtained by the 2D CFD results. The design data account 3D source losses by empirical correlations (Kacker-Okapuu loss model), which justifies the good agreement with the 3D CFD results.



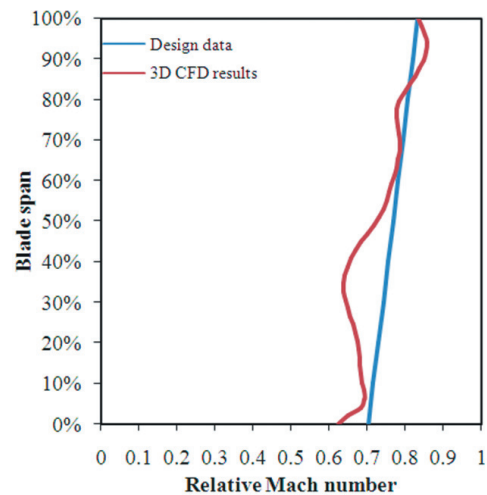
Leading edge



Leading edge



Trailing edge



Trailing edge

Figure 5. Absolute Mach number distribution at stator blade.

Figure 6. Relative Mach number distribution at rotor blade.

The mass flow rate of design data is 4% greater than that predicted by the 3D CFD results. This result is consistent, as suggested by Dorney (2003). The factor that influenced the mass flow in the design data is the model limitation that uses one-dimensional equations of motion to predict the flow quantities in the turbine. While the factor that influenced the mass flow in the 3D CFD results is attributed to the fillets consideration that reduces the flow passage area.

As can be shown by Fig. 7, there is flow separation in the suction side of the rotor blade, which reduces the pressure ratio across the turbine (Tomita and Barbosa (2011)). This behavior can justify the difference between pressure ratios of the 3D CFD results and the design data in Table 2.

The present study also focused on the performance maps of the first-stage axial turbine. These maps were constructed at design rotational speed (22,600 rpm).

The curves shown in Fig. 8 present similar overall tendency, but 3D CFD results are in better agreement with Denton loss model when compared with 2D CFD ones. It can be observed that the turbine efficiency is plotted against different operating points and the curves are shifted due to the limitations of each method.

It is also noted that turbine efficiency is nearly constant over a wide range of pressure ratio (up to 1.75 for Denton loss model, e.g.). This happens because the accelerating nature of the flow allows the blade to operate over a large range of incidence flow angles, without increasing the loss, as discussed by Saravanamuttoo *et al.* (2001).

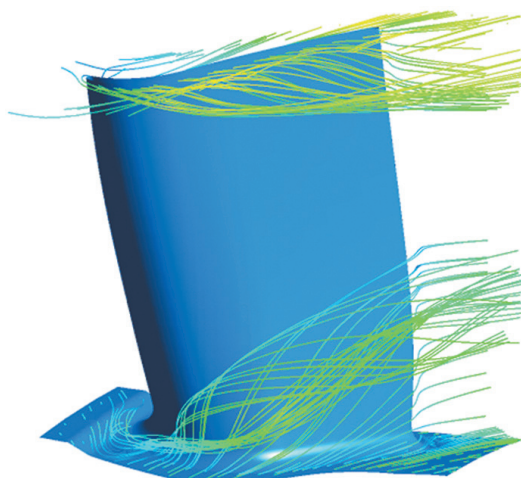


Figure 7. Streamlines of the secondary flow.

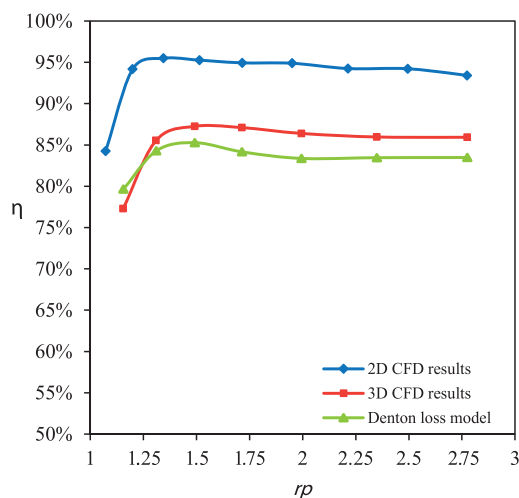


Figure 8. First stage turbine performance map of efficiency as a function of the pressure ratio.

Figure 9 presents values for the corrected mass flow at each operation condition. The 2D CFD corrected mass-flow was not presented because the simulation was evaluated at stage middle surface.

Besides, Fig. 9 shows that the corrected speed lines tend to horizontal ones. This condition is reached at higher pressure ratios, which produce choking conditions at some point in the turbine stage. Depending on the design, choking may occur in the nozzle throats or in the annulus outlet from the turbine. Figure 10 shows choked regions in the stator blades, indicated by yellow isosurfaces.

Choking conditions happen when the pressure ratio is increased at a given rotational speed. The flow field develops supersonic velocities, which usually form shock waves in the nozzle throats, resulting in shock wave losses.

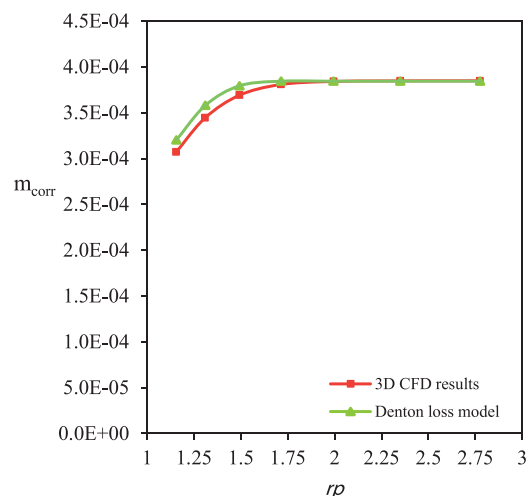


Figure 9. First stage turbine performance map of corrected mass flow as a function of the pressure ratio.

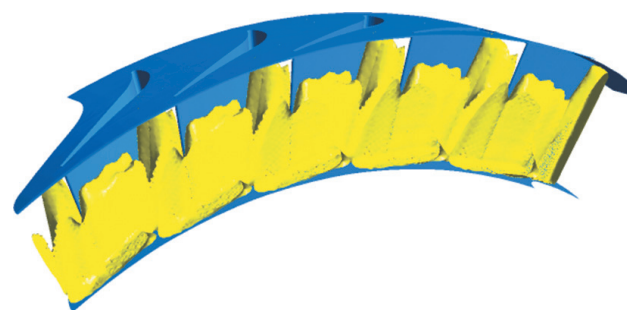


Figure 10. Yellow isosurfaces of mach ≥ 1 at stator blades.

CONCLUSIONS

A series of computational simulations have been conducted to provide pretest performance for the first-stage axial turbine. The flow and performance quantities predicted using the mean line loss model code and 2/3 D Navier-Stokes equations adopted in the numerical simulation showed reasonable agreement.

The results provided by the comparison of the flow parameters, such as Mach number and total pressure, showed good agreement observed by the general tendency of the curves. This concludes that the 3D CFD results are consistent with mean line analysis used in the conceptual design of the turbine in study.

The agreement between performance maps curves generated by the CFD simulation and mean line loss model using Denton loss model, showed that the numerical simulation, which solves the conservations equations and turbulence model, is consistent with loss model adopted. The disposition of curves generated by 2D and 3D simulations showed the degree of fidelity that each model depicts the losses. As would be expected, the 3D CFD results are in better agreement with Denton loss model when

compared with 2D CFD ones. This happens because the 3D CFD results and Denton loss model account 3D flow patterns in performance quantities, which are not accounted in the 2D simulation.

The advantage of using the CFD simulation, when comparison is made against mean line loss model code, is the large number of analysis that the CFD tool is capable of providing, such as flow visualization showed by Figs. 7 and 10.

ACKNOWLEDGMENTS

The authors thank *Vale Soluções em Energia* (VSE) for the support to this research.

REFERENCES

- ANSYS, 2009a, “Fluent 12.0 theory guide”, Canonsburgh, PA, Cap. 18.
- ANSYS, 2009b, “Ansys CFX-solver theory guide: release 12.0”, Canonsburgh, PA, Cap. 9.
- Denton, J.D., 1993, “The 1993 IGTI scholar lecture: loss mechanisms in turbomachines”, *Journal of Turbomachinery*, Vol. 115, pp. 621-656.
- Denton, J.D., Xu, L., 2002, “CFD for turbomachinery aerodynamic design”, London: [s.n.], IMECHE Grand review of CFD.
- Dorney, D.J. *et al.*, 2003, “Off-design performance of a multi-stage supersonic turbine”, In: *Aerospace Sciences Meeting and Exhibit, 41th Aerospace Sciences Meeting & Exhibit, Reno, Proceedings...Washington, DC: AIAA; 2003.*
- Eulitz, F., Engel, K., 1997, “Numerical investigation of wake interaction in a low pressure turbine”, In: *33rd AIAA/ASME/SAE/ASEE Joint Propulsion Conference And Exhibit, Seattle, WA. Proceedings...Washington, DC: AIAA.*
- Fletcher, C.A.J., 1991, “Computational techniques for fluid dynamics”, 2. ed., Berlin, Springer-Verlag, Vol. 2, Cap. 1.
- Fortuna, A.O., 2000, “Técnicas computacionais para dinâmica dos fluidos: conceitos básicos e aplicações”, São Paulo, Edusp.
- Haglund, F., Elmergaard, B., 2009, “Methodologies for predicting the part-load performance of aero-derivative gas turbines”, *Energy*, Vol. 34, pp. 1484-1492.
- Hess, R., 2006, “Estudo comparativo de método de análise de desempenho de turbinas axiais”, PhD Thesis, Instituto Tecnológico de Aeronautica, São José dos Campos, S.P., Brazil, 105p.
- Javaherchi, T., 2010, “Review of spalart-allmaras turbulence model and its modifications”, Hartford, CT, Rensselaer Polytechnic Institute.
- Menter, F.R., 2003, “Turbulence modelling for turbomachinery”, *QNET CFD Network Newsletter*, Vol. 2, No. 3, pp. 10-13.
- Murari, S. *et al.*, 2011, “CFD aerodynamic CFD validation of a two-stage high pressure turbine”, In: *ASME TURBO EXPO, 2011, Vancouver, British Columbia, Proceedings... New York, ASME.*
- Pecnik, R. *et al.*, 2005, “Numerical Investigation of the Secondary Flow of a Transonic Turbine Stage Using Various Turbulence Closures”, In *ASME Turbo Expo 2005, Power for Land, Sea and Air, Reno-Tahoe, ASME Paper GT2005-68754.*
- Saravanamuttoo, H.I.H., 1992, “Overview on basis and use of performance prediction methods”, Carleton University Ottawa, AGARD Advisory Report, LS-183.
- Saravanamuttoo, H.I.H. *et al.*, 2001, “Gas turbine theory”, 5. ed., Harlow, Prentice Hall, 2001, Cap. 7.
- Spalart, P.R., Allmaras, S.R.A., 1992, “One equation turbulence model for aerodynamic flow”, Washington, DC, AIAA, 1992. (AIAA Paper 92-0439).
- Tannehill, J.C. *et al.*, 1997, “Computational fluid mechanics and heat transfer”, 2. ed. Philadelphia, Taylor & Francis, 1997, pp. 272-280.

Tomita, J.T., Barbosa, J.R., 2011, "Influence of inflow turbulence intensity variations in an axial turbine using 3D RANS computations", In: International Congress of Mechanical Engineering, 21, Natal, Proceedings...Rio de Janeiro, ABCM, 2011.

Toussaint, C. *et al.*, 1997, "Comparison of steady and unsteady 3D viscous flow computations through a transonic turbine stage", Chatillon, FR, Office National d'Etudes et de Recherches Aeronautiques (ONERA), ONERA-TAP-97-147.

Welch, G.E., 2011, "Computational assessment of the aerodynamic performance of a variable-speed power turbine for large civil tilt-rotor application", Cleveland, Ohio, NASA John H. Glenn Research Center at Lewis Field, 2011.

Wilcox, D.C., 1993, "Turbulence modeling for CFD", 2. ed., La Canada, CA, DCW Industries.